Broad low-frequency phonon resonance for increased across-tube heat transport

Lin Qiu [ORCID], Fengcheng Li, Ning Zhu, and Yanhui Feng[*]

School of Energy and Environmental Engineering, University of Science and Technology Beijing, Beijing 100083, China

Xiaoliang Zhang [ORCID][†]

Key Laboratory of Ocean Energy Utilization and Energy Conservation of Ministry of Education,
School of Energy and Power Engineering, Dalian University of Technology, Dalian 116024, China

Xiaohua Zhang [ORCID][‡]

Innovation Center for Textile Science and Technology, Donghua University, Shanghai 201620, China

The poor heat conduction between carbon nanotubes (CNTs) has become a severe obstacle, hindering the applications for thermal management. Considering that the across-tube heat transport is limited by the small fraction of low-frequency phonons (LFPs), it is of great necessity to develop a strategy to excite LFPs without modifying the tube contacts. Herein, a mechanism of LFP resonance is proposed by assigning soft long-chain polymers (e.g., polyurethane and polyethylene) to the groove sites of contacted CNTs. The resonance takes places at multiple points and in wide ranges of frequencies and wave vectors, originating from the rich low-frequency vibrations localized at the soft segments of the polymer. More excited phonons lead to an extraordinary improvement on the across-tube heat conductance, by a factor of 79%, which opens a route to develop advanced CNT-based thermal functional materials.

I. INTRODUCTION

Rapid size miniaturization and power density boost in microelectronic devices bring about striking heat accumulation around the devices, strongly deteriorating their performance and shortening their service life. Thus, heat dissipation has become the key issue that restricts the advances of microelectronics [1–3]. Carbon nanotubes (CNTs) possess an ultrahigh thermal conductivity of $\sim$6000 W m^{-1} K^{-1} [4,5] and are regarded as some of the most feasible approaches to solve the heat dissipation problem. However, when they are assembled toward large-scale practical applications (e.g., CNT bundles, fibers, films, and foams), the poor across-tube heat conduction and the presence of CNT ends lead to an orders-of-magnitude decline in the overall performance of heat transport [6]. This is generally ascribed to the weak phonon coupling based on the van der Waals (vdW) intertube interaction [7,8]. To pave the way to boost the across-tube heat conduction, enhancing the intertube coupling and thus the phonon matching has been considered the most effective solution.

From the perspective of intertube interaction, a variety of methods have been proposed to optimize the across-tube heat conduction, such as the shortening of intertube distance, extending the overlap length, enlarging the contact area, wrapping polymer chains around CNTs, and so forth [8–13]. Typically, the interfacial thermal conductance per unit tube

length (G_L) at room temperature can be improved from 0.0036 up to 0.08 W m^{-1} K^{-1} by optimizing the geometric arrangement [8,14–16]. Clearly, these methods can benefit the phonon coupling and thus heat conduction between CNTs. However, the improvement is quite limited, as the conduction in these cases is primitively based on the enlarged vdW interaction area, rather than the resonance-based energy exchange between the phonons of contacted CNTs [17]. In principle, as the low-frequency phonons (LFPs) are of great importance to carry heat energy [11,18–20], it is crucial to activate the excitation and resonance of LFPs of the carbon atoms at CNT contacts. Thus far, it has been reported that the optical pulses [21], hammer impact (mechanical pulses) [22], heat pulses [23], and friction [24,25] can effectively excite LFPs in CNTs. Furthermore, by experimentally anchoring metal nanoparticles or molecule chains into CNT fibers, LFP excitation has been observed with the Raman scattering characterization, where the thermal conductivity of the fiber was remarkable enhanced by $\sim$75% [26–29]. However, it requires external excitation energies to stimulate the LFPs for the above approaches. Thus, toward a stably enhanced across-tube heat transport, it is necessary to increase the density of states at the LFP region, which can lead to a strengthened resonating (coupling) between these LFPs for contacted CNTs. As a possible solution, polymer chains that possess rich LFP modes can be used as agents to open channels for the LFP coupling.

Therefore, a schematic of such a mechanism can be represented by Fig. 1. Without the presence of a polymer, there is only one channel to conduct heat between CNTs via phonon coupling. When polymer chains are introduced at the groove sites, additional CNT-polymer-CNT channels are established,

[*]yhfeng@me.ustb.edu.cn
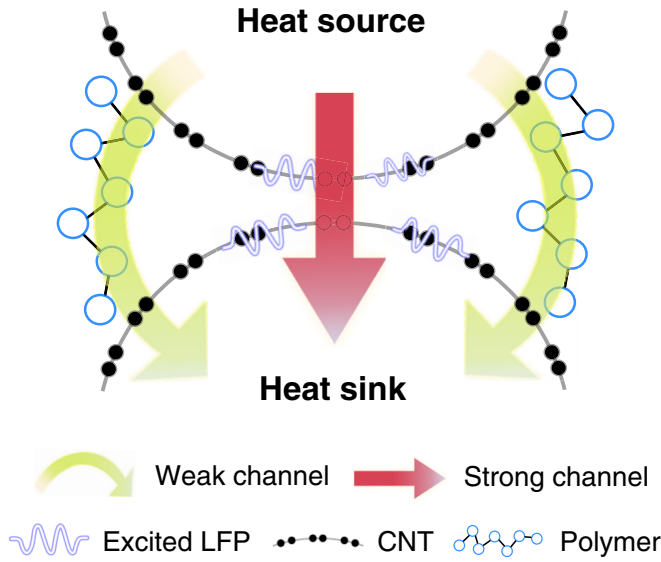[†]zhangxiaoliang@dlut.edu.cn
[‡]zhangxh@dhu.edu.cn

Heat source

FIG. 1. Schematic of polymer-broadened heat transport channels for contacted carbon nanotubes (CNTs).

and the conventional CNT-CNT channel is also affected by the polymer. By considering the low thermal conductivity of the polymer, the newly added CNT-polymer-CNT channels are the weak ones, while the CNT-CNT channel can be greatly broadened once the phonon density is evidently increased.

Herein, we show such broadening effect can be indeed realized by long-chain polymers, such as polyurethane (PU) and polyethylene (PE). The rich soft segments in the polymers can resonate well with CNTs in a rich range of LFPs and thus broaden the CNT-CNT heat transport channel at least by 35.5%, based on the chain length and number of chains. This modulation effect is reminiscent of the gating effect in field-effect transistors, where the electric transport is enhanced by the more excited charge carriers. In this paper, we provide a strategy to construct a composite structure for high-performance thermal functional materials.

II. METHODS AND SIMULATIONS

Owing to the hard and soft segments in PU molecular chains [Fig. 2(a)], the atoms can intrinsically vibrate at different frequencies, providing rich possibilities to resonate with their contacting nanotube. The PU chains considered in this paper were built up by randomly connecting monomer 4, 4′-methylene diphenyl diisocyanate (MDI, hard segment) with polytetrahydrofuran (PTMEG, soft segment, containing 12 1,4-butanediol units) using a urethane bond (intermediate) [30], as schematically shown in Fig. 2(a). Different repeating numbers for the MDI-PTMEG units, $n = 1$ to 10, were investigated to evaluate the effect of the molecular chain length. (Nearly identically, such an effect was also shown by increasing the number of chains m.) Figure 2(b) illustrates a typical PU molecular chain with $n = 1$. The PU-modulated CNT contacts were modeled by using BIOVIA Materials Studio 2019 (19.1.0.2353). As the simplest composition, two PU chains with $n = 1$ were initially manually placed at the two groove sites of two contacted CNTs [Fig. 2(c)]. The CNTs,

both (20,20) with a length of 123 Å, were arranged in parallel, and the axial overlap length and the intertube distance were set to be 40 and 3.4 Å, respectively.

The LAMMPS package was used to conduct the nonequilibrium molecular dynamics (NEMD) simulations [31]. Two segments (10 Å) along the z direction on both sides of the CNT edge are set as thermal insulation walls [Fig. 2(d)], and the nonperiodic boundary conditions are employed for all directions of the simulated box. The adaptive intermolecular reactive empirical bond order (AIREBO) was used to describe the interactions between carbon atoms in the two CNTs. For the PU molecules that contain C, H, N, and O atoms, the COMPASS force field was used, which contains the description of bonded terms (bond length, bond angle, and dihedral angle) and nonbonded interaction terms [32]. For the PE molecules composed of C and H atoms, the AIREBO potential was directly used for convenience, as this potential has been developed to describe hydrocarbons as well [33]. Finally, for the intermolecular vdW interactions, the Lennard-Jones (LJ) potentials were used, namely, $V_{LJ}(r) = 4\varepsilon[(\sigma/r)^{12} - (\sigma/r)^6]$, with a cutoff distance of 10 Å. The parameters are $\sigma = 3.000$ Å and $\varepsilon = 0.0028$ eV between two C atoms, 3.025 Å and 0.0021 eV between C and H, 4.230 Å and 0.0031 eV between C and N, and 3.620 Å and 0.0033 eV between C and O.

Before the NEMD simulation, the steepest descent method was utilized to minimize the energy of the system. Then a Nosé-Hoover thermostat [34] was used to adjust the system temperature to 300 K, within 6×10^5 time steps (0.5 fs per step). In the following simulations, the two regions of heat source and heat sink, with a length of 10 Å and far away from the contact [see Fig. 2(d)], were modeled by using the Jund-Julline method [35] to conduct a 0.5 eV/ps heat flow from the heat source to the sink. When the simulation time exceeds 1.0 ns and the temperatures of the two segments [marked as 1 and 2 in Fig. 2(d)] do not change with time, a stable temperature difference ΔT is established at the contact [Fig. 2(e)]. Therefore, the stable configuration at 1.6 ns was used to calculate the interfacial thermal conductance G_L, normalized by the contact length [Fig. 2(f)]:

$$G_L = \frac{J}{L_{\text{overlap}} \Delta T}, \tag{1}$$

where J denotes the heat flow, as determined by the energy $\Delta\epsilon$ subtracted from the atoms in heat sink and added to the atoms in heat source, and ΔT denotes the temperature difference, calculated from the average temperatures for carbon atoms within the overlap region [marked as segment 1 and segment 2 in Fig. 2(d)] in the two contacted CNTs.

III. RESULTS AND DISCUSSION

A. Across-tube heat conduction

The present computational model has been widely applied to evaluate the interfacial heat conductance. For the pure (20,20) CNT contact considered in this paper, when a heat flow $J = 0.5$ eVps^{-1} is applied, the temperature difference becomes $\Delta T \approx 263$ K [Figs. 2(e) and 2(f)], and $G_L = 0.076$ W m^{-1} K^{-1} according to Eq. (1). This is a typical value for CNT contacts [8,14–16]. For example, for two parallel
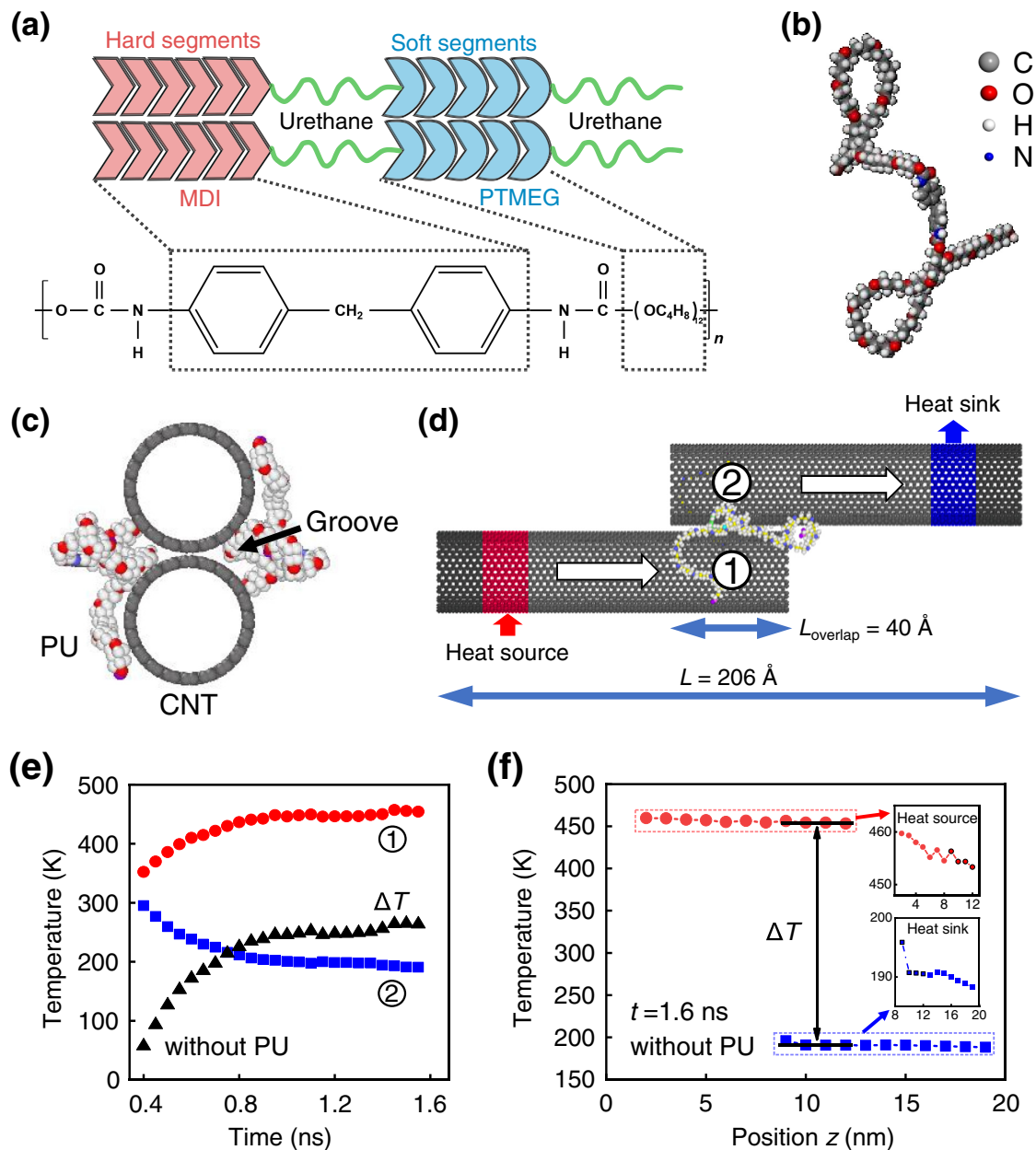
FIG. 2. Simulation model for across-tube heat transport. (a) and (b) Schematics of molecular structures for polyurethane (PU). (c) and (d) PU-modulated intertube interface. Two PU chains are placed at the two groove sites. Heat source and heat sink are at the ends of the bottom and top tubes, respectively. The overlapped segments are marked as 1 and 2. (e) Temperatures of regions 1 and 2 and their difference are plotted as functions of time. (f) The steady temperature profile along the two tubes at $t = 1.6$ ns. Inset highlights temperature variability in carbon nanotubes (CNTs).

(5,5) CNTs, G_L is ~ 0.005 W m^{-1} K^{-1} [8] and increases up to 0.038 W m^{-1} K^{-1} when they are interlaced with each other to enlarge the contact area [15], and the G_L between two interlaced (10,0) CNTs is up to 0.079 W m^{-1} K^{-1} [15].

When PU chains are introduced to cover the groove sites, there is a remarkable increase in G_L, from 0.076 to 0.10 W m^{-1} K^{-1} [Fig. 3(a)], indicating a broadening effect on the across-tube channels for heat conduction. Then with increasing the PU chain length, G_L goes into a slowly climbing stage; it just increases from 0.10 to 0.136 W m^{-1} K^{-1}, by a value close to the first jump, when the chain length becomes tenfold, i.e., $n = 10$. In another way, with increasing the num-ber of PU chains up to $m = 8$ without changing the chain length ($n = 1$), G_L also renders a similarly slow and linear increase up to 0.13 W m^{-1} K^{-1} [Fig. 3(b)]. Differently, the conductance grows up with increasing the number of chains at a more rapid rate than the case of increasing the chain length. For example, at $n = 1$ and $m = 8$, $G_L = 0.130$ W m^{-1} K^{-1}, while at $n = 10$ and $m = 2$, $G_L = 0.136$ W m^{-1} K^{-1}. Further-more, due to the random Brownian motion of the polymers during the simulation [Fig. 3(c)], as in the error bar results of $n = 2, 10$, or $m = 6$, it can be found that the soft segments are gathered in the grooves can bring a slightly better effect, while the hard segments have no effect. According to these results,
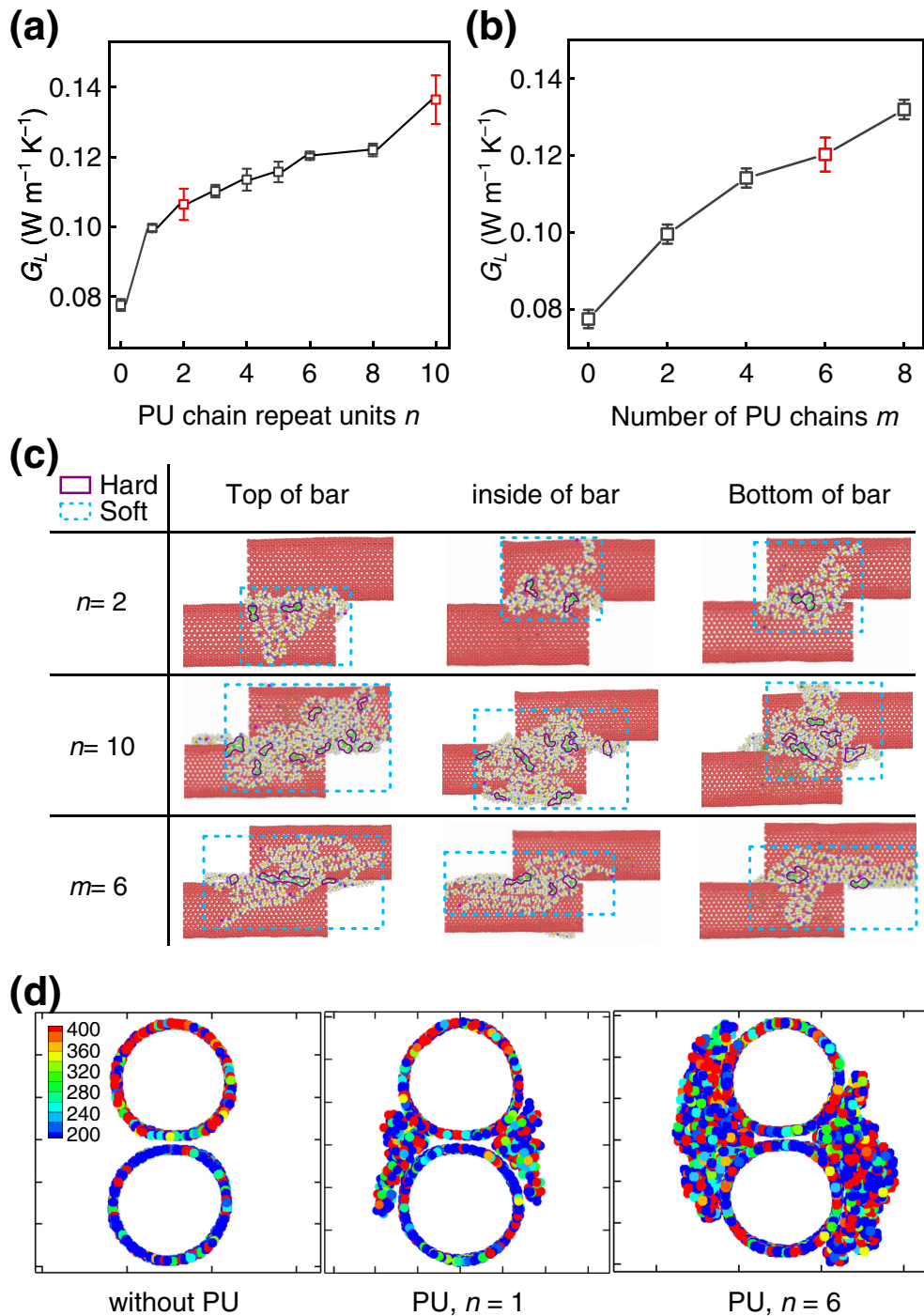
FIG. 3. Enhanced across-tube thermal conduction by polyurethane (PU) covering. (a) G_L as a function of PU chain length, represented by the number of repeating units n. (b) Intertube interfacial thermal conductance (G_L) as a function of the number of PU chains (m), by fixing the chain length parameter as $n = 1$. (c) The effects of soft and hard segments on G_L at different adsorption positions at a steady state. The results correspond to the red error bars in (a) and (b), respectively. (d) Snapshots showing the temperature distribution in the contacted carbon nanotubes (CNTs) without PU covering and with PU covering at chain lengths of $n = 1$ and 6, respectively.

the adsorption sites of the polymer chains have little effect on the across-tube thermal conductance enhancement. Consequently, the PU covering induces the decrease in ΔT between the two tubes, from ≈ 260 K for the uncovered contact to ~ 190 and 160 K when the PU length is $n = 1$ and 6, respectively, as indicated by the snapshots shown in Fig. 3(d). Clearly, the presence of PU chain induces a jump in G_L, and adjusting the

PU length or number, the across-tube heat conduction can be nearly doubled.

In such problems, atomic simulations for larger temperature differences show that the calculated interfacial conductance is related to the temperature difference itself. Therefore, by inputting smaller heat flow (0.4, 0.3, and 0.2 eVps^{-1}) compared with the current case (0.5 eVps^{-1}) to

TABLE I. The upgrade rate of interfacial thermal conductance under different heat flux.

J (eV ps^{-1})	$(n = 0, m = 0)$		$(n = 1, m = 2)$		Upgrade rate (%)
	$\Delta T_{(0)}$ (K)	$G_L^{(0)}$ (W m^{-1} K^{-1})	$\Delta T_{(2)}$ (K)	$G_L^{(2)}$ (W m^{-1} K^{-1})	
0.5	263	0.076	200	0.100	31.50
0.4	211	0.076	157	0.102	34.67
0.3	154	0.078	120	0.099	27.91
0.2	108	0.074	77	0.104	40.70

the contacted CNTs, it is found that the temperature differences without PU $\Delta T_{(0)}$ decrease to 211, 154, and 108 K from 263 K, respectively (temperature difference with PU $\Delta T_{(2)}$ from 200 K to 157, 120, 77 K, respectively). Therefore, the degree of interfacial heat transfer enhancement via polymer addition is 34.67, 27.91, and 40.70%, respectively (see Table I). This value oscillates slightly compared with the rate of increase value at 0.5 eVps^{-1} (31.5%), due to the random position of the polymer at stabilization. This proves that the enhancement of the interfacial conductance by the polymers does not depend on the temperature difference.

As PU itself is likely a thermal insulator as compared with CNT, the CNT-PU-CNT pathway may not be the major channel for heat transport. Furthermore, such assigning of polymer molecules on the groove sites does not evidently affect the intertube contact area, indicating that there should be a special source for the sudden boost of G_L. According to Fig. 1, one can divide the heat conduction into two possible ways, namely, the heat energy exchange by phonon coupling between CNTs and the additional heat transport pathways of CNT-PU-CNT. The former one is the direct and strong transport from CNT to CNT and is referred as G_{direct}. The latter one is the indirect channel via the CNT-PU-CNT pathway, i.e., G_{indirect}. Generally speaking, the indirect channel is a weak one, yet its contribution still should be determined as quantitatively as possible. To do so, the total conductance was evaluated for the below five considerations:

(1) Without PU covering, the total conductance is $G_{\text{direct}}^{(0)} = 0.076$ W m^{-1} K^{-1}.

(2) A short PU ($n = 1$) at one groove site ($m = 1$), $G_{\text{direct}}^{(1)} + G_{\text{indirect}} = 0.090$ W m^{-1} K^{-1}.

(3) Two chains ($n = 1$) at two groove sites ($m = 2$), $G_{\text{direct}}^{(2)} + 2G_{\text{indirect}} = 0.100$ W m^{-1} K^{-1}; here, the two indirect channels are considered the same as that in case (2).

(4) A long PU ($n = 10$) at one groove site ($m = 1$), $G_{\text{direct}}^{(3)} + G_{\text{indirect}}^* = 0.103$ W m^{-1} K^{-1}.

(5) Two chains ($n = 10$) at two groove sites ($m = 2$), $G_{\text{direct}}^{(4)} + 2G_{\text{indirect}}^* = 0.136$ W m^{-1} K^{-1}.

By subtracting cases (2) and (3), we obtain $G_{\text{indirect}} + [G_{\text{direct}}^{(2)} - G_{\text{direct}}^{(1)}] = 0.010$ W m^{-1} K^{-1}. Clearly, $G_{\text{indirect}} < 0.010$ W m^{-1} K^{-1}, as more PU chains strengthen the direct channel more. Therefore, by further comparing cases (1) and (2), the strengthening magnitude to the direct channel $[G_{\text{direct}}^{(1)} - G_{\text{direct}}^{(0)}] > 0.004$ W m^{-1} K^{-1}. Note that the short PU molecular chain has a very limited contact with the CNT; thus, the direct channel is not broadened very much. Nevertheless, it is clear that the indirect channel does not contribute much to the total heat conductance.

Then with increasing the chain length, the strengthening effect becomes higher. By comparing cases (2) and (4), the total conductance is found to further increase by 0.013 W m^{-1} K^{-1} due to the longer chain length. For an extreme assumption that half of such further increase is from the indirect channel, the highest value for G_{indirect}^* should be just the sum of G_{indirect} and the half increase, namely, $0.010 + \frac{0.013}{2} = 0.0165$ W m^{-1} K^{-1}. Therefore, by following a similar analysis, one can get $G_{\text{direct}}^{(3)} > 0.0865$ and $G_{\text{direct}}^{(4)} > 0.103$ W m^{-1} K^{-1}.

Clearly, the above analysis is the worst consideration. Even though, from case (1) to (5), where the total conductance is increased by 78.9% (from 0.076 to 0.136 W m^{-1} K^{-1}), the direct conductance is increased at least by 35.5% (from 0.076 to >0.103 W m^{-1} K^{-1}).

B. Enhanced LFPs in CNT

The remarkable increase in G_{direct} should be ascribed to the enhanced intertube phonon coupling. To make it clear, the vibrational density of states (VDOS) of a particular group of atoms (α) in Fig. 4(a) was calculated from the Fourier transform of the velocity autocorrelation function:

$$Z^\alpha(t) = \frac{\langle \vec{v}_i^\alpha(0) \cdot \vec{v}_i^\alpha(t) \rangle}{\langle \vec{v}_i^\alpha(0) \cdot \vec{v}_i^\alpha(0) \rangle}, \tag{2}$$

where $\vec{v}_i^\alpha$ is the velocity vector of atom i of a particular group α, and t is the correlation time. Note that the LFP vibration <20 THz contributes greatly to the thermal conduction of CNTs [18,36]. Thus, the difference of VDOS characteristics in the low-frequency range has a direct correlation to promote the boost of G_{direct}.

Overall, as shown in Fig. 4(b), the difference in VDOS at high frequencies (>30 THz) is quite small for the carbon atoms at the contact (interfacial atoms) and far away from the contact (noninterfacial atoms), while there is a clear enhancement at the low-frequency region of 3–15 THz. Here, the overlapped 40 Å segment was divided into two groups, namely, the interfacial carbons and noninterfacial carbons. The former contains the atoms with a minimum distance <5 Å with the atoms in the other CNT, identical to the two bottom atom rows of the upper CNT, and the latter contains those atoms as far as possible away from the contact, corresponding to the two top atom rows in the present (20,20) CNT [Fig. 4(a)]. As the LFPs carry the heat energy farther [18], this VDOS change indicates the phonon coupling between the two tubes has been enhanced by the PU covering.

To explore which phonons are involved in the enhancement of across-tube thermal transport, a two-dimensional (2D) Fourier transform was performed on $Z^\alpha(t)$ of the interfacial
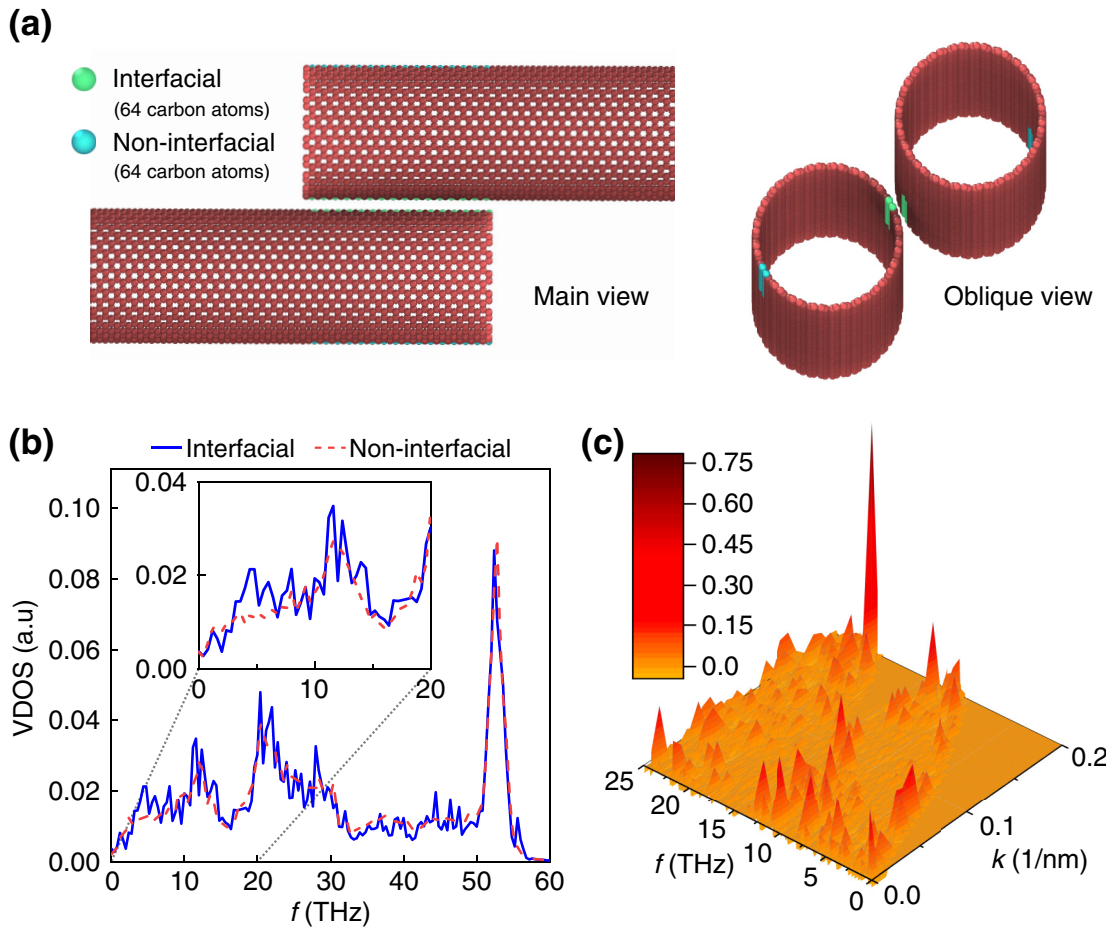
(a)

(b)

(c)

FIG. 4. Enhanced low-frequency phonon (LFP) vibrations by polyurethane (PU) covering. (a) Schematic diagram of the positions and numbers of interfacial and noninterfacial carbon atoms. (b) Comparison of the vibrational density of states (VDOS) between the carbon atoms at and far away from the intertube contact. (c) The difference between the two-dimensional (2D) Fourier transform $I(k, f)$ of carbon nanotube (CNT) vibration with and without the PU chains, in a frequency range of 0–25 THz. The PU chain length is $n = 1$ in (b) and (c).

atoms in dimensions of time and space to generate the phonon power spectrum $I(k, f)$ [37], see Fig. 4(c). The major observation is that the excited phonons mostly locate within 0–15 THz and possess a wide range of wave vector k. These phonons are the breathing modes with low rotational symmetries or with an angular momentum number of 2, 3, 4, ... [24,25]. These breathing modes are not excited at the Γ point ($k = 0$) because the PU-induced phonon excitation is localized rather than the uniform excitation around the whole circumference. Note that there is also a strong excitation at $f \approx 22$ THz and $k \approx 0.2$ nm^{-1}, the edge of Brillouin zone, indicating an effect of Umklapp processes. Nevertheless, as the summation of the enhanced VDOS within the low-frequency range (e.g., 3–15 THz) is stronger than this Umklapp excitation, these multipoint excitations should be the main contribution to the enhanced across-tube heat transport.

C. Origination of phonon resonance

To understand how the PU chain affects the LFP excitation, a similar vibrational analysis was also conducted for different PU segments, see Fig. 5(a). Here, the PU chain was divided

into four segments, namely, G1 and G2 for the segments at the groove site and O1 and O2 out of the groove. Here, O1 and G1 are the two soft segments (six 1,4-butanediol units) connected by carbon-oxygen bond c4o-o2e [the atom types are defined in the COMPASS force field, see Fig. 5(b)], and G2 is composed of two intermediates and a hard segment, connected with G1 by a c3-o2s bond. Finally, O2 is a longer soft segment (12 1,4-butanediol units) linked to G2 with an o2s-c3 bond. It is found that the VDOS spectrum for the O1 and O2 segments do not change much in the frequencies <20 THz after being absorbed at CNT surfaces. On the contrary, apparent changes appear in the vibrational characteristics for the segments at the groove site. Specifically, the G1 segment laying along the groove direction renders a boost of LFPs <4 THz, while the G2 segment clustering in the groove exhibits an evident excitation within 8–12 THz. The G2 segment possesses the unique hard feature because the N atom (strongly hybridized with the neighboring C atoms) in the intermediate and the benzene rings in the hard segment lead to high rigidity. The G1 segment is much softer and thus can provide sufficient low-frequency matching with the contacted CNTs.
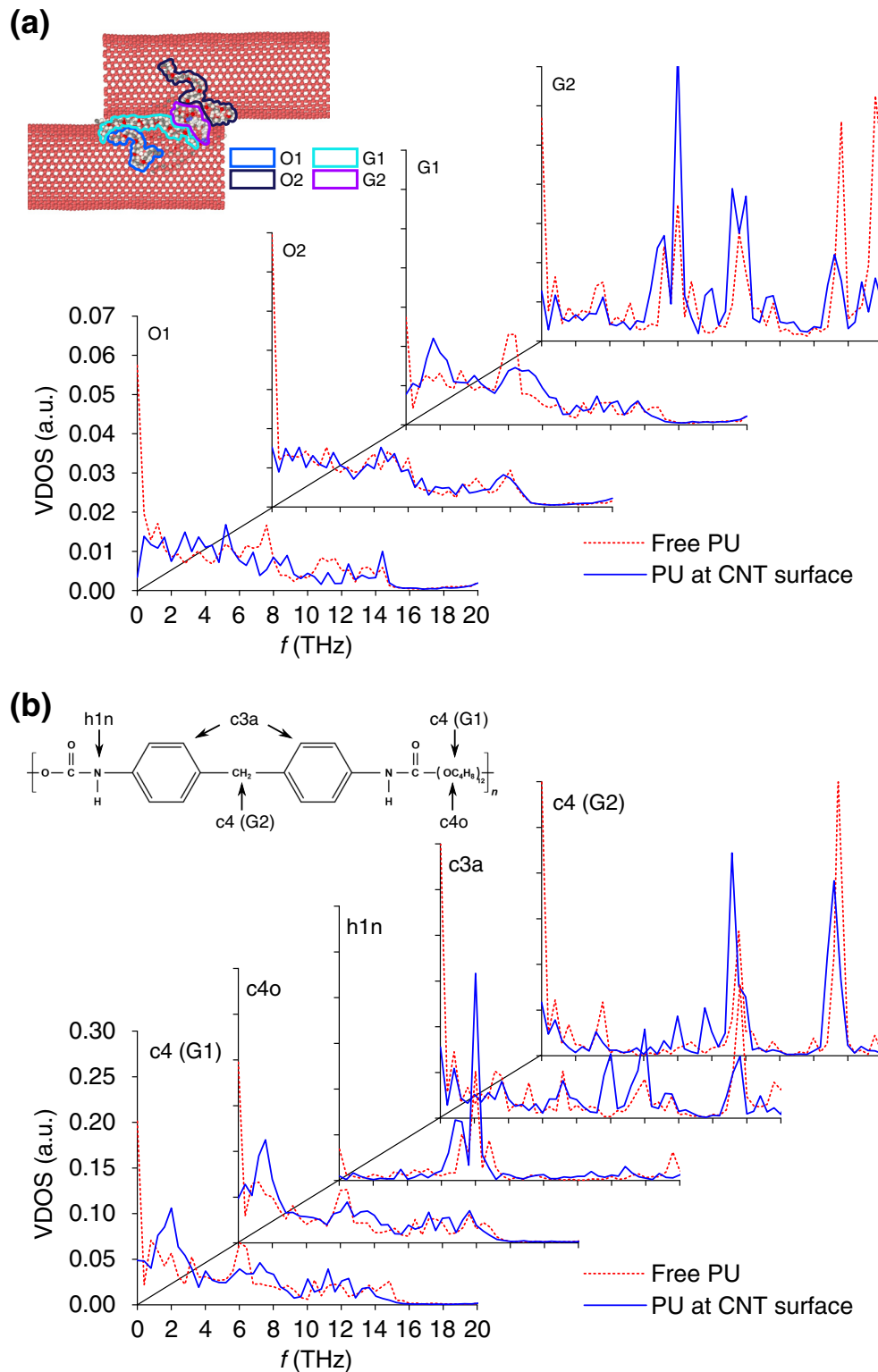
FIG. 5. Vibration analysis for different segments and atom groups in a polyurethane (PU) chain. (a) The PU chain was divided into four segments, including the G1 and G2 at the groove site and O1 and O2 out of the groove. Here, $n = 1$. (b) The c4, c4o, and h1n atoms (in G1) and the c3a and c4 atoms (in G2) situated at the CNT groove site as compared with the corresponding key atoms in an isolated PU.

The resonance between PU and the CNT depends on the subtle molecular structures and can be represented by a series of key atoms in the chain whose vibration behavior changes greatly after interacting with CNTs. Five atoms in the G1 and G2 segments [Fig. 5(b)] are found to show the evident change

in the vibrations. The h1n, c3a, and c4 atoms in G2 all exhibit vibration enhancement at 8–12 THz and a certain vibration suppression at 18–20 THz. The c4 and c4o atoms in G1 render evident vibration enhancement <4 THz after contacting with the CNT. The key atoms containing C atoms in G1 (c4 and
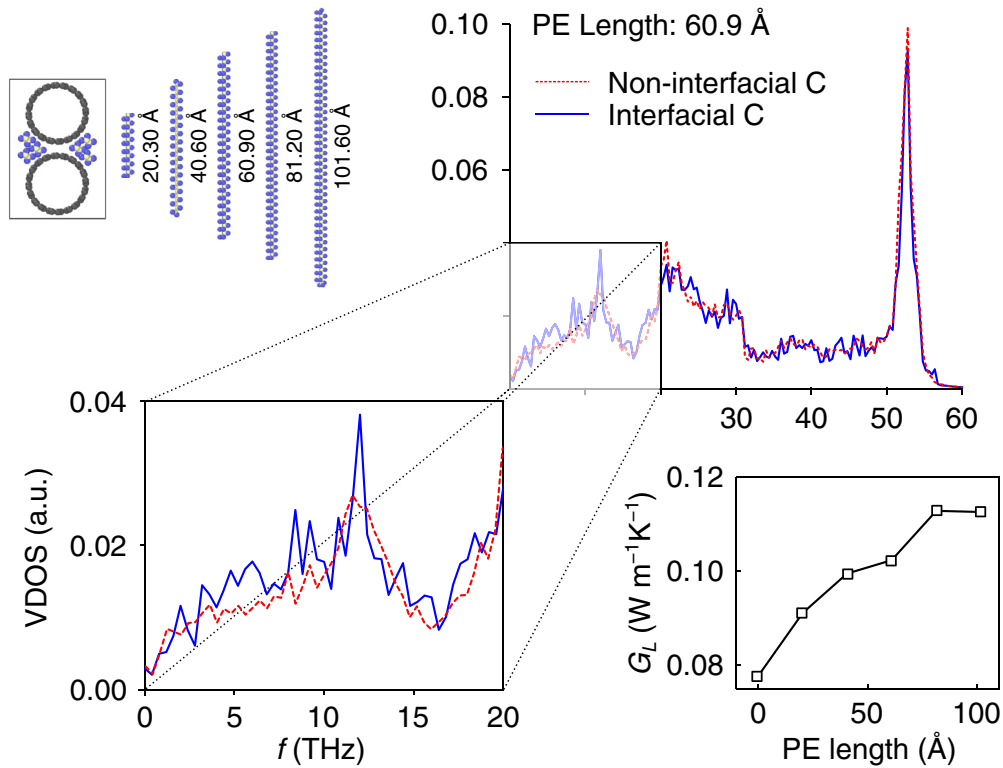
FIG. 6. Effect of polyethylene (PE) covering on G_L and vibrational density of states (VDOS). The vibration analysis was conducted for the simulation with a PE length of 60.9 Å.

c4o) can produce obvious resonance excitation between PU and the CNT, which is the main cause for boost of the across-tube heat transport.

Therefore, from the above observation and analysis, an opening effect can be established based on the resonance-strengthened density of states (DOS) of LFPs, leading to the widened intertube heat transport channels. Interestingly, this is quite like the gating effect in field-effect transistors where a gate voltage can widen or open the conductive channels. PU can be an efficient candidate, as it contains rich soft segments which can vibrate at low frequencies.

D. Ubiquity of phonon resonance

From the above analysis on the different segments of the PU molecular chain, it is speculated that this opening/broadening mechanism is a ubiquitous phenomenon for other long-chain polymers. To verify this, PE chains with different lengths were also investigated, see Fig. 6. Quite like Fig. 3(a), with increasing the PE length from 10.15 to 101.60 Å, G_L is also significantly improved from 0.076 up to $0.091-0.113\,\mathrm{W\,m^{-1}\,K^{-1}}$. By performing the vibrational analysis on the interfacial and noninterfacial carbon atoms, a similar difference in VDOS can be observed within 2.5–12 THz. These results are very consistent with the PU investigation, indicating a strategy to enhance the thermal conductivity of CNT assembly materials and CNT-based composite materials.

Interestingly, there have been a series of investigations on the interfacial heat transport between nanocarbon contacts and the possible strengthening effect like in this paper, see Fig. 7.

The conductance values were normalized according to the contact area in each study. Overall, the intrinsic interfacial conductance strongly depends on the type of nanocarbon, its nanostructure (e.g., chirality, diameter, and number of layers), and the spacing distance. By introducing guest materials onto the interfaces, remarkable enhancements have been observed, both experimentally and theoretically. The most common method is changing the diameter or distance between the CNTs [8,15]. Due to the complexity of the experimental operation, the diameter of CNTs and the overlap length and area are generally much larger, leading to larger experimental interfacial thermal conductance than the simulation results [16]. When guest materials are introduced to CNT-CNT contact, the conductance is remarkably increased. For example, by using iodine molecule chains to increase the conductance from 37.1 to $42.3\,\mathrm{MW\,m^{-2}\,K^{-1}}$ [27,29] and gold nanoparticles from 8 to $12.8\,\mathrm{MW\,m^{-2}\,K^{-1}}$ [26]. In addition to nanoclusters, polymer chains also have been experimentally reported, e.g., by controlling the bismaleimide (BMI) mass fraction to be 30%, and using electro-curing to optimize the CNT/BMI contacts, it has been observed that the conductance can be increased from 20 to $141\,\mathrm{MW\,m^{-2}\,K^{-1}}$ [10]. However, polymers wrapping around thick bundles of CNTs typically result in reduced heat conductance because, in most cases, there is overloading of polymers in CNT assemblies. It might be beneficial for high mechanical performance, but the overloaded polymers can block the heat transport channels between CNTs. For example, at a fraction of epoxy >50 wt. %, the room temperature thermal conductivity decreases from 42 to $7.5\,\mathrm{W\,m^{-1}\,K^{-1}}$ for an aligned CNT film [38]. For the CNT/BMI composite films with aligned CNTs, at a BMI fraction of 65 wt. %, it might
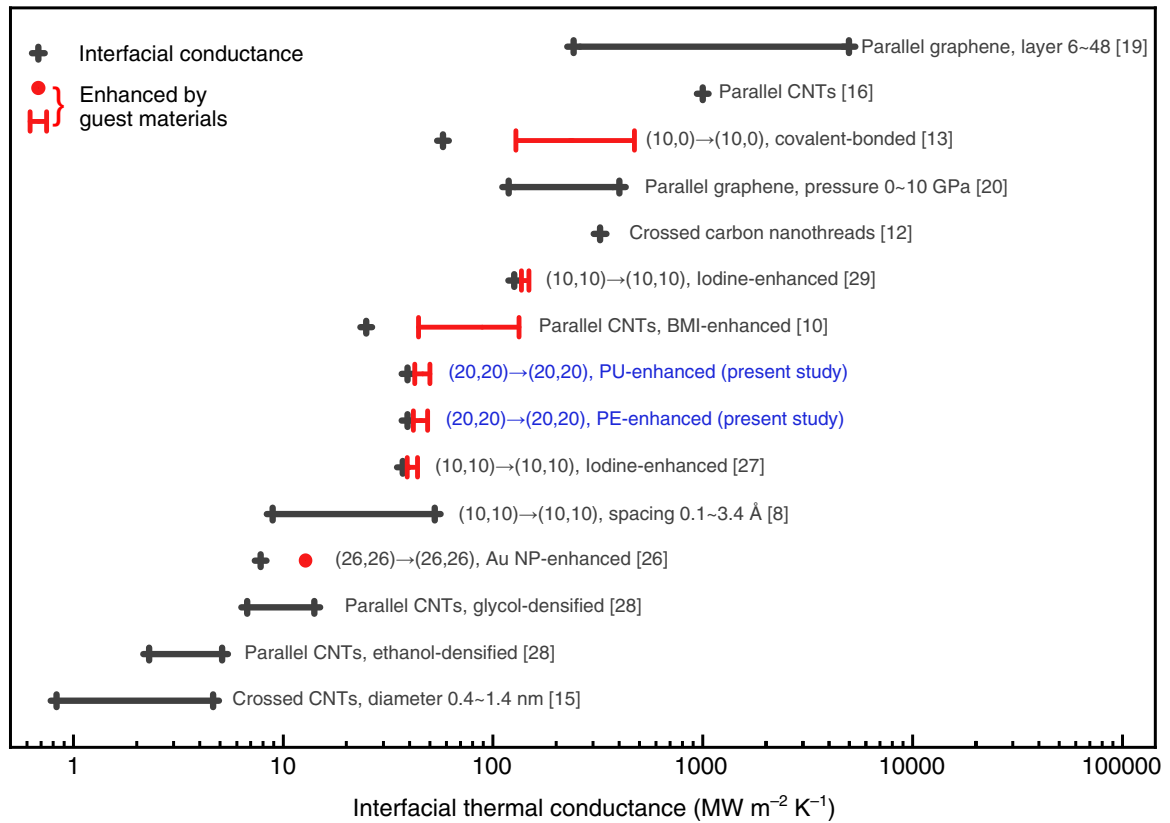
FIG. 7. Interfacial thermal conductance between nanocarbon contacts and the strengthening by using guest materials.

recover the thermal conductivity of the pure CNT film when the tube length is sufficiently long [39]. Overall, in practical situations, the impregnation of the polymer is usually not conducive to heat transfer, but it can be controlled by changing its content.

This phenomenon is also observed in the contact structures of other nanocarbon materials, such as graphene and carbon nanothreads [12,19,20,40]. Unlike the sp^2 bonding in a CNT, the carbon nanothreads have an ultrathin sp^3 bond with a fully hydrogenated surface [12], and thus, the conductance of crossed carbon nanothreads with the same tubular structure is two orders of magnitude larger than the crossed CNTs. The multilayer graphene contacts or the parallel graphene contacts under pressure exhibit higher conductance [19,20]. In addition, it has been found that covalent bonding can provide a larger increase in the interfacial conductance [13]. However, it is necessary to look into a method of enhancing the interfacial conductance from another aspect, that is, only relying on the guest particles to excite more LFPs to participate in the interfacial energy transport.

Clearly, the thermally insulating polymers can be used to modulate the across-tube heat conduction, depending on the way the polymers are introduced into the CNT materials. When the polymers are confined at the groove sites, without changing the contact geometry of the CNTs, the polymer-CNT LFP resonance can open a wider channel for heat transport. Otherwise, for most cases, the polymers are simply introduced to fill the voids between CNTs, which can

just induce a slight improvement of the across-tube heat conduction [40], or they are even overloaded to degrade the CNT contacts and thus block the transport channels. The present resonance-based mechanism can guide the structural design for high-performance thermal management materials.

IV. CONCLUSIONS

Thermally insulating polymers are found to be able to improve the across-CNT heat transport, based on the resonance-enhanced VDOS for the LFPs in a CNT. This is an opening/broadening effect like the gate-controlled conductive channels for charge carriers in field-effect transistors. In this paper, we provide a strategy to design CNT-based thermal functional materials.

ACKNOWLEDGMENTS

[1] W. Lee, K. Kim, W. Jeong, L. A. Zotti, F. Pauly, J. C. Cuevas, and P. Reddy, Heat dissipation in atomic-scale junctions, Nature (London) **498**, 209 (2013).

[2] Y. Zhang, H. Han, N. Wang, P. Zhang, Y. Fu, M. Murugesan, M. Edwards, K. Jeppson, S. Volz, and J. Liu, Improved heat spreading performance of functionalized graphene in micro-electronic device application, Adv. Funct. Mater. **25**, 4430 (2015).

[3] L. Qiu, N. Zhu, Y. Feng, E. E. Michaelides, G. Żyła, D. Jing, X. Zhang, P. M. Norris, C. N. Markides, and O. Mahian, A review of recent advances in thermophysical properties at the nanoscale: From solid state to colloids, Phys. Rep. **843**, 1 (2020).

[4] J. Hone, M. Whitney, C. Piskoti, and A. Zettl, Thermal conductivity of single-walled carbon nanotubes, Phys. Rev. B **59**, R2514(R) (1999).

[5] S. Berber, Y.-K. Kwon, and D. Tománek, Unusually High Thermal Conductivity of Carbon Nanotubes, Phys. Rev. Lett. **84**, 4613 (2000).

[6] A. N. Volkov, R. N. Salaway, and L. V. Zhigilei, Atomistic simulations, mesoscopic modeling, and theoretical analysis of thermal conductivity of bundles composed of carbon nanotubes, J. Appl. Phys. **114**, 104301 (2013).

[7] S. T. Huxtable, D. G. Cahill, S. Shenogin, L. Xue, R. Ozisik, P. Barone, M. Usrey, M. S. Strano, G. Siddons, M. Shim, and P. Keblinski, Interfacial heat flow in carbon nanotube suspensions, Nat. Mater. **2**, 731 (2003).

[8] H. Zhong and J. R. Lukes, Interfacial thermal resistance between carbon nanotubes: Molecular dynamics simulations and analytical thermal modeling, Phys. Rev. B **74**, 125403 (2006).

[9] Z. Xu and M. J. Buehler, Nanoengineering heat transfer performance at carbon nanotube interfaces, ACS Nano **3**, 2767 (2009).

[10] L. Qiu, P. Guo, X. Yang, Y. Ouyang, Y. Feng, X. Zhang, J. Zhao, X. Zhang, and Q. Li, Electro curing of oriented bismaleimide between aligned carbon nanotubes for high mechanical and thermal performances, Carbon **145**, 650 (2019).

[11] L. Qiu, X. Zhang, Z. Guo, and Q. Li, Interfacial heat transport in nano-carbon assemblies, Carbon **178**, 391 (2021).

[12] H. Zhan, G. Zhang, X. Zhuang, R. Timon, and Y. Gu, Low interfacial thermal resistance between crossed ultra-thin carbon nanothreads, Carbon **165**, 216 (2020).

[13] V. Varshney, S. S. Patnaik, A. K. Roy, and B. L. Farmer, Modeling of thermal conductance at transverse CNT-CNT interfaces, J. Phys. Chem. C **114**, 16223 (2010).

[14] S. Maruyama, Y. Igarashi, Y. Taniguchi, and Y. Shibuta, Molecular dynamics simulations of heat transfer issues in carbon nanotubes, in Proceedings of the First International Symposium on Micro and Nano Technology (Honolulu, Hawaii, USA, 2004).

[15] Y. Chalopin, S. Volz, and N. Mingo, Upper bound to the thermal conductivity of carbon nanotube pellets, J. Appl. Phys **105**, 084301 (2009).

[16] J. Yang, S. Waltermire, Y. Chen, A. A. Zinn, T. T. Xu, and D. Li, Contact thermal resistance between individual multiwall carbon nanotubes, Appl. Phys. Lett. **96**, 023109 (2010).

[17] P. A. Greaney and J. C. Grossman, Nanomechanical Energy Transfer and Resonance Effects in Single-Walled Carbon Nanotubes, Phys. Rev. Lett. **98**, 125503 (2007).

[18] Z. Yao, J.-S. Wang, B. Li, and G.-R. Liu, Thermal conduction of carbon nanotubes using molecular dynamics, Phys. Rev. B **71**, 085417 (2005).

[19] Z. Wei, Z. Ni, K. Bi, M. Chen, and Y. Chen, Interfacial thermal resistance in multilayer graphene structures, Phys. Lett. A **375**, 1195 (2011).

[20] C. Liu, Z. Wei, W. Chen, K. Bi, J. Yang, and Y. Chen, Pressure effects on the thermal resistance of few-layer graphene, Phys. Lett. A **380**, 248 (2016).

[21] A. Gambetta, C. Manzoni, E. Menna, M. Meneghetti, G. Cerullo, G. Lanzani, S. Tretiak, A. Piryatinski, A. Saxena, R. L. Martin, and A. R. Bishop, Real-time observation of nonlinear coherent phonon dynamics in single-walled carbon nanotubes, Nat. Phys. **2**, 515 (2006).

[22] E. Ghavaminezhad, M. Mahnama, and N. Zolfagharia, The effects of van der Waals interactions on the vibrational behavior of single-walled carbon nanotubes using the hammer impact test: A molecular dynamics study, Phys. Chem. Chem. Phys. **22**, 12613 (2020).

[23] L. Chen and S. Kumar, Thermal transport in double-wall carbon nanotubes using heat pulse, J. Appl. Phys. **110**, 074305 (2011).

[24] X. H. Zhang, G. E. Santoro, U. Tartaglino, and E. Tosatti, Dynamical Chiral Symmetry Breaking in Sliding Nanotubes, Phys. Rev. Lett. **102**, 125502 (2009).

[25] X. H. Zhang, G. E. Santoro, U. Tartaglino, and E. Tosatti, Dynamical phenomena in fast sliding nanotube models, Philos. Mag. **93**, 922 (2013).

[26] L. Qiu, H. Zou, X. Wang, Y. Feng, X. Zhang, J. Zhao, X. Zhang, and Q. Li, Enhancing the interfacial interaction of carbon nanotubes fibers by Au nanoparticles with improved performance of the electrical and thermal conductivity, Carbon **141**, 497 (2019).

[27] L. Qiu, H. Zou, N. Zhu, Y. Feng, X. Zhang, and X. Zhang, Iodine nanoparticle-enhancing electrical and thermal transport for carbon nanotube fibers, Appl. Therm. Eng. **141**, 913 (2018).

[28] L. Qiu, X. Wang, D. Tang, X. Zheng, P. M. Norris, D. Wen, J. Zhao, X. Zhang, and Q. Li, Functionalization and densification of inter-bundle interfaces for improvement in electrical and thermal transport of carbon nanotube fibers, Carbon **105**, 248 (2016).

[29] H. Zou, Y. Feng, L. Qiu, and X. Zhang, Effect of the loading amount and arrangement of iodine chains on the interfacial thermal transport of carbon nanotubes: A molecular dynamics study, RSC Adv. **10**, 44196 (2020).

[30] J. Goclon, T. Panczyk, and K. Winkler, Investigation of the interfacial properties of polyurethane/carbon nanotube hybrid composites: A molecular dynamics study, Appl. Surf. Sci. **433**, 213 (2018).

[31] S. Plimpton, Fast parallel algorithms for short-range molecular dynamics, J. Comput. Phys. **117**, 1 (1995).

[32] H. Sun, COMPASS: An *ab initio* force-field optimized for condensed-phase applications overview with details on alkane and benzene compounds, J. Phys. Chem. B **102**, 7338 (1998).

[33] S. J. Stuart, A. B. Tutein, and J. A. Harrison, A reactive potential for hydrocarbons with intermolecular interactions, J. Chem. Phys **112**, 6472 (2000).

[34] D. J. Evans and B. L. Holian, The Nose-Hoover thermostat, J. Chem. Phys **83**, 4069 (1985).

[35] P. Jund and R. Jullien, Molecular-dynamics calculation of the thermal conductivity of vitreous silica, Phys. Rev. B **59**, 13707 (1999).

[36] J. Li and H. Shen, Effects of fullerene coalescence on the thermal conductivity of carbon nanopeapods, Mol. Phys. **116**, 1297 (2018).

[37] P. Tangney, M. L. Cohen, and S. G. Louie, Giant Wave-Drag Enhancement of Friction in Sliding Carbon Nanotubes, Phys. Rev. Lett. **97**, 195901 (2006).

[38] P. Gonnet, Z. Liang, E. S. Choi, R. S. Kadambala, C. Zhang, J. S. Brooks, B. Wang, and L. Kramer, Thermal conductivity of magnetically aligned carbon nanotube buckypapers and nanocomposites, Curr. Appl. Phys. **6**, 119 (2006).

[39] X. Wang, Q. Jiang, W. Xu, W. Cai, Y. Inoue, and Y. Zhu, Effect of carbon nanotube length on thermal, electrical and mechanical properties of CNT/bismaleimide composites, Carbon **53**, 145 (2013).

[40] J. Zhang, C. Jiang, D. Jiang, and H. Peng, Nano-engineering thermal transport performance of carbon nanotube networks with polymer intercalation: A molecular dynamics study, Phys. Chem. Chem. Phys. **16**, 4378 (2014).